Modeling Laser Plasma Interactions for Enhanced Target Normal Sheath Acceleration and Surface Modification

Research Thesis

Presented in partial fulfillment of the requirements for graduation with *research distinction* in the undergraduate colleges of The Ohio State University

By
Nashad Rahman

The Ohio State University
April 2021

Project Advisors:
Dr. Douglass Schumacher and Dr. Christopher Orban
Department of Physics

Acknowledgements

I would like to thank both of my research advisors, Dr. Douglass Schumacher and Dr. Christopher Orban, for their continued support and for always taking the time to explain complex ideas in ways that I can comprehend. I want to thank all the graduate students, post docs, and staff who have taken time out of their very busy lives to help me over the years, including Joe Smith, Alexander Klepinger, Pedro Spingola, Preston Pozderac, Nick Czapla, Anthony Zingale, Derek Nasir, German Tiscareno, and Becky Daskalova. I would also like to thank Dr. Linn Van Woerkom for introducing me to the field of Plasma Physics.

I would also like to thank my parents and sister for their everlasting support, encouragement, and enthusiasm for the work that I do. Lastly, I thank my roommates who have made final year of undergrad so much more enjoyable, even during a global pandemic.

Contents

Chapter 1

Modeling Laser Plasma Interactions at Intensities Which Cause Surface Modifications

1.1 Introduction

There are many interesting phenomena which occur when laser light interacts with matter. Much research has been done to explore how ultra-high intensity lasers will destroy a target and much research has been done to explore lower intensity lasers which do not modify the surface of a target at all. Between these regimes, there is much to be explored regarding lasers with intensities great enough to modify the surface of a target, but not great enough to drastically alter the target. Of particular interest is to observe how an irradiated target will radiate electromagnetic waves at frequencies other than the frequency of the incoming laser.

The difficulty in these simulations lies in ability to faithfully simulate the particle interactions happening in "warm" plasmas. This regime of physics is often called Warm Dense Matter (WDM) and occurs at temperatures lower than what is typically considered in plasma physics. In this state, matter is dense and particles are often too strongly coupled to be modeled as a plasma, which have much weaker coupling and particle interaction. However, the matter is also too hot to be modeled as condensed matter.

Plasma physics is generally modeled through the use of Particle-In-Cell (PIC) simulations. The PIC method in its most basic form does not address particle interactions like collisions and scattering. Many common collision models exist, which are then implemented into PIC codes, however, most of these models are not able to accurately model warm dense matter. To address this, we used a novel collision algorithm as described in Russell and Schumacher [7].

1.2 Simulation setup

We used the LSP code in implicit mode to perform 2D3V simulations [11]. We used an implicit field advance and and implicit particle pusher. A 3 µm by 3 µm copper was

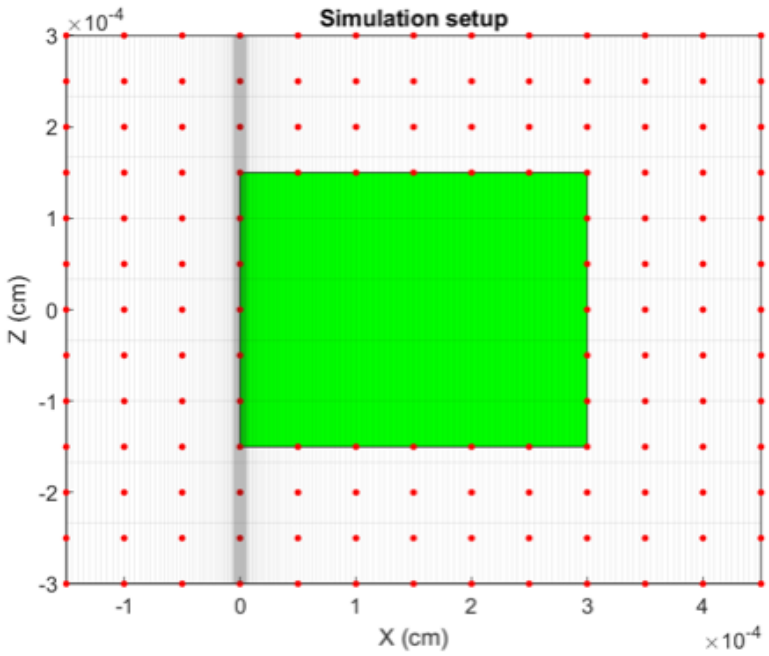

Figure 1.1: Simulation set up for surface modification simulations. Illustrated in green is the target. The entire grid is shown and the gray lines represent the cell boundaries (some are omitted in the z direction). The red dots mark the positions of the probes. The laser pulse enters from the left boundary and travels right. Figure courtesy of A. Klepinger.

irradiated by a laser pulse with an intensity of 5 $\times 10^{13}$ W cm^{-2}. The laser pulse had a wavelength of 1 µm, a pulse duration of 40 fs (FWHM) and a spot size of 1 µm. The grid changed drastically between various simulations, but the "baseline" model was set up to be 6 µm by 6 µm with 272 by 120 cells. The target was placed in the center such that there was 1.5 µm between the target and the boundary of the simulation in all directions. The cells in the x-direction were varied in order to provide greater resolution at the leading surface of the target. The baseline simulation had 9 copper nuclei macroparticles per cell and 100 electron macroparticles per cell, all of which were initialized at 0.025 eV. The particles were all fully ionized at the start of the simulation and thus no ionization model was necessary. Probes were placed throughout the grid in order to read out the electric and magnetic fields in all three coordinate dimension. These probes are used to analyze the response from the irradiated target.

1.3 Challenges with initial simulations

To understand the behavior of the target after being irradiated, we looked to observe the frequency response by taking the Fourier transform of various probes throughout our simulation. The probes measured the electric and magnetic fields in the x, y, and z directions, however our analysis focused heavily on the y-component of the magnetic field since any electromagnetic wave polarized in the plane of the simulation would have a magnetic field in

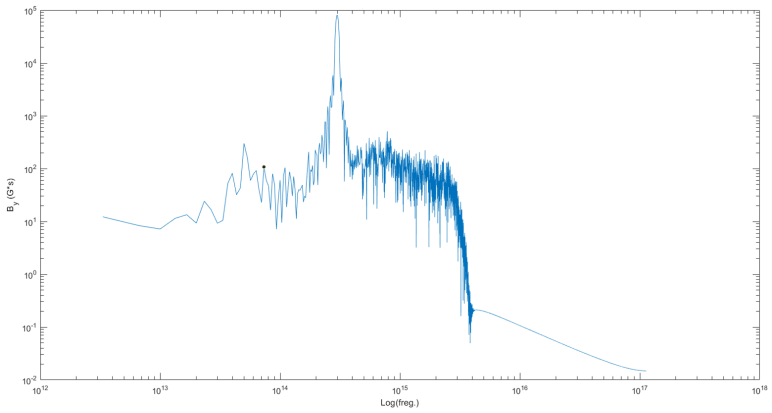

Figure 1.2: Initial frequency response from simulations. The low frequency response around 50 Thz was thought to be emitted by the target, but in reality this was a result of numerical errors. The peak at 300 THz is from the incoming laser pulse and is not of particular interest. The high frequency response at frequencies above 300 THz is noise and also not of particular interest. Figure courtesy of A. Klepinger.

the y-direction (out of the plane of the simulation). Fig. 1.2 shows the frequency response of the y-component of the magnetic field at a point 0.5 µm in front of the target, in the path of the laser ($-0.5\,\mu m$, $0\,\mu m$). We observed significant frequency responses in the lower end of the frequency spectrum and initially believed this frequency to have been emitted from from the irradiated target. However, after a test to see what noise would be present without even having a target, we found that similar responses were present even in the absence of a target.

Further investigation showed that significant computational errors were occurring with the leading edge of our laser pulse. The leading edge was seemingly increasing in intensity and reflecting back and forth between the right boundary of the simulation and the left boundary. Our first attempts to fix this issue was to implement various other boundary conditions. Originally, an outlet boundary was used on the left boundary where the laser entered and a conductor boundary was used elsewhere. These conductor boundaries were then changed to outlet boundaries, periodic boundaries, and various forms of Perfectly-Matched-Layers, but the low frequency response at $5 * 10^{13}$ hz remained, as shown in the left panel of Fig 1.3.

This problem was ultimately solved by altering the wave envelope from a sine squared envelope to a Gaussian envelope. This allowed for a more gradual turn on for the laser pulse. The more gradual increase eliminated the issues from the start of the pulse reflecting off of the boundaries. The length of the leading and trailing end of the envelope was increased to further allow for a smoother turn on, thereby reducing noise as shown in the left panel of Fig. 1.3.

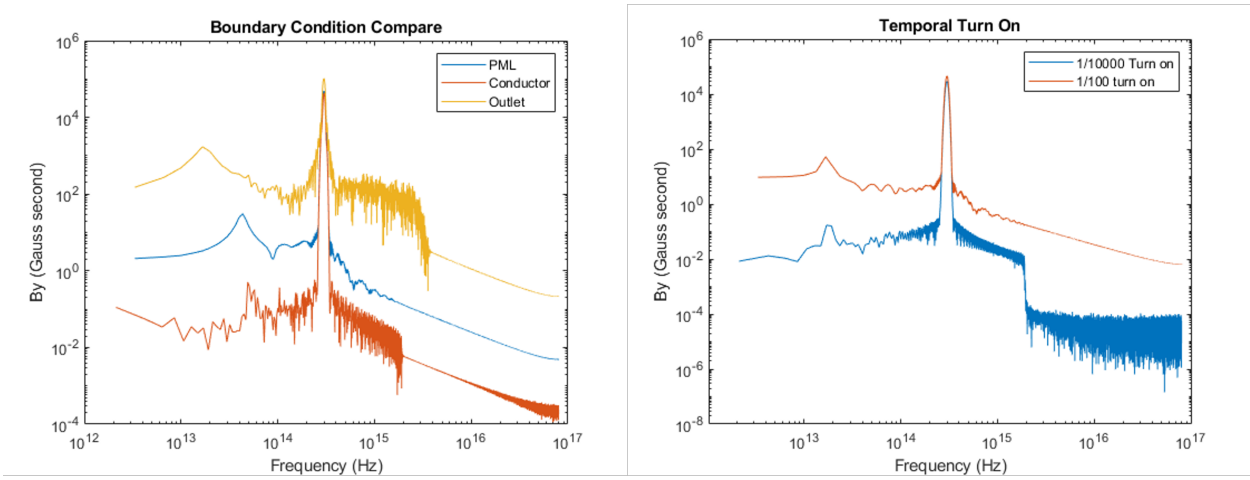

Figure 1.3: (left) Comparison of various boundary conditions used in attempts to mitigate issues caused the the front end of the pulse reflecting off of the boundaries. The sine squared envelope was used in each of these simulations. The Conductor boundaries was similar to that in Fig 1.2, and the PML used was the Convolutional PML. (right) Frequency response from after altering the envelope to be a Gaussian pulse. The lines show the frequency response of a beam with a Gaussian envelope where the tail was extended to be 1/10,000 the magnitude (blue) and 1/100 the magnitude (red). Figures courtesy of A. Klepinger.

1.4 Pushing to longer time regimes

After the laser interacts with the target, the target continues to evolve. Reaching longer simulation times is of great interest to allow us to better understand the next stages of the laser damage process. However, as the time limit of these simulations is increased, other challenges arise. Firstly, longer time scales become more computationally expensive as a greater number of timesteps must be simulated. Longer time scales may also lead to numerical errors from instabilities which become less reasonable and more prominent over time. In order to scale this simulation into the picosecond or nanosecond regime, we must eliminate the noise which may be causing instabilities and decrease the computational cost of our simulation. One way to approach this issue is to stop the simulation in it's current form, and then restart with the particle positions and momenta still in tact but removing the high frequency noise of the fields. Our current efforts to reduce the high frequency noise are to run a segment of the simulation with time biasing, or to remove the fields all together at the end of the initial part of the simulation, and initialize the fields of the second part of the simulation with a static field solve.

Chapter 2

Enhanced Target Normal Sheath Acceleration Using a Double Pulse Configuration

2.1 Introduction

Energetic ions have useful applications in a wide variety of applications [2, 8, 10, 3, 6], however, conventional accelerators can be very large and costly which greatly limits this technology being used in application. Ultra-intense lasers may be a promising source of high energy ions that are more affordable and compact. In general, increasing the laser intensity increases the peak energy of these ions, however, as the intensity of a laser increases, so too does the cost of the laser. This leads us to be interested in increasing the efficiency of laser-ion acceleration without increasing the laser intensity.

One phenomena used to accelerate ions with lasers is Target Normal Sheath Acceleration (TNSA) in which laser excitation causes electrons at the front of a target to be accelerated to the back of the target and create an electron cloud which is then able to accelerate the ions in the target [12, 9]. An approach to increase the efficiency of TNSA is described in Ferri, Siminos, and Fülöp [4] which shows through 2D3v Particle in Cell (PIC) simulations that irradiating a target using two pulses of half intensity can increase the peak ion energy drastically when compared to one pulse of full intensity. The authors find that two pulses arriving at 45 degrees away from normal achieves the optimal results.

There are a number of concerns which must considered before this phenomena can be demonstrated experimentally. Previous explorations of this phenomena have been done under ideal conditions where the lasers arrive at the target at the exact same time and focused to the exact same spot on target. However, such ideal conditions are rare in experiment and thus raises interest in the robustness of this effect. Specifically, we are interested to see the effect of spatial, temporal, and phase offsets on the peak energy of the ions. A key concern is also whether this phenomena can be seen at intensities lower than those described in Ferri, Siminos, and Fülöp [4] and with thinner targets of a different material.

2.2 Simulation setup

We used the implicit mode of the LSP code and performed 2D3v simulations. [11] We used an implicit field advance and and implicit particle pusher. The laser pulse had a pulse duration of 42 fs (FWHM) and a spot size of 2.2 µm (FWHM) with a sine squared envelope. The intensity of the laser in the single pulse simulations was 5×10^{18} W cm^{-2} while the intensity for the double pulse simulation was 2.5×10^{18} W cm^{-2}, thus keeping the total energy equal for both simulations. The entire grid was 28 microns by 28 microns and consisted of 2800 by 2800 cells. A 0.46 µm thick ethylene glycol target was placed such that it was angled 45 degrees to the simulation grid. This allowed for one laser pulse to irradiate the target from above and the other from the left, both incoming at 45 degrees to normal. Each cell with the target was initialized with 9 particles of protons, electrons, carbon, and oxygen, for a total of 36 particles in each cell. Each particle was initialized to a temperature of 1 eV. The electron density of the target was initialized at 10^{23} cm^{-3} with all other species being adjusted to ensure a neatral target at the beginning of the simulation. Field ionization was done using the ADK model [1]. The simulations were run for 1 ps and had time steps of 20 as.

2.3 Results from temporally and spatially aligned pulses

Fig 2.1 shows the electric field component in the plane of the simulation normal to the target. The single pulse simulation is shown on the top panel and the double pulse simulation is shown on the bottom panels. The right column of the figure shows 50 fs after the start of the simulation at which point the laser pulses are just beginning to interact with the target. The laser pulse entering from the top boundary of the simulation is polarized in the $+x$ direction and the pulse entering from the left boundary is polarized in the $-z$ direction. Both of these polarizations are easily seen as the field component normal to the target is being shown.

The middle panels of Fig 2.1 show the fields at 100 fs after the start of the simulation. The laser pulse is not strongly interacting with the the target and much of it is reflected off the target. Interestingly, there is constructive interference occurring in both the single pulse and the double pulse simulations. The sheath fields on the back side of the target are weaker and more asymmetric for the single pulse simulation than for the double pulse simulation.

The right panels of Fig 2.1 show the fields at 150 fs after the start of the simulation. At this point, the laser pulses have passed the target and have mostly left the simulation grid. The sheath field in the double pulse simulation remains stronger and more symmetric than the sheath field of the single pulse simulation. The centers of these targets have also expanded as part of the TNSA process.

Fig. 2.2 shows the energies and positions of a random selection of protons at 450 fs after the start of the simulation. The left panel is for the single pulse and the right panel is for the double pulse simulations. At 450 fs, enough time has passed for the difference in ion energies is particularly apparent, but not enough time has passed for the protons to begin leaving the grid. This plot shows that the maximum proton energy is noticeably higher in the double pulse that in the single pulse simulation.

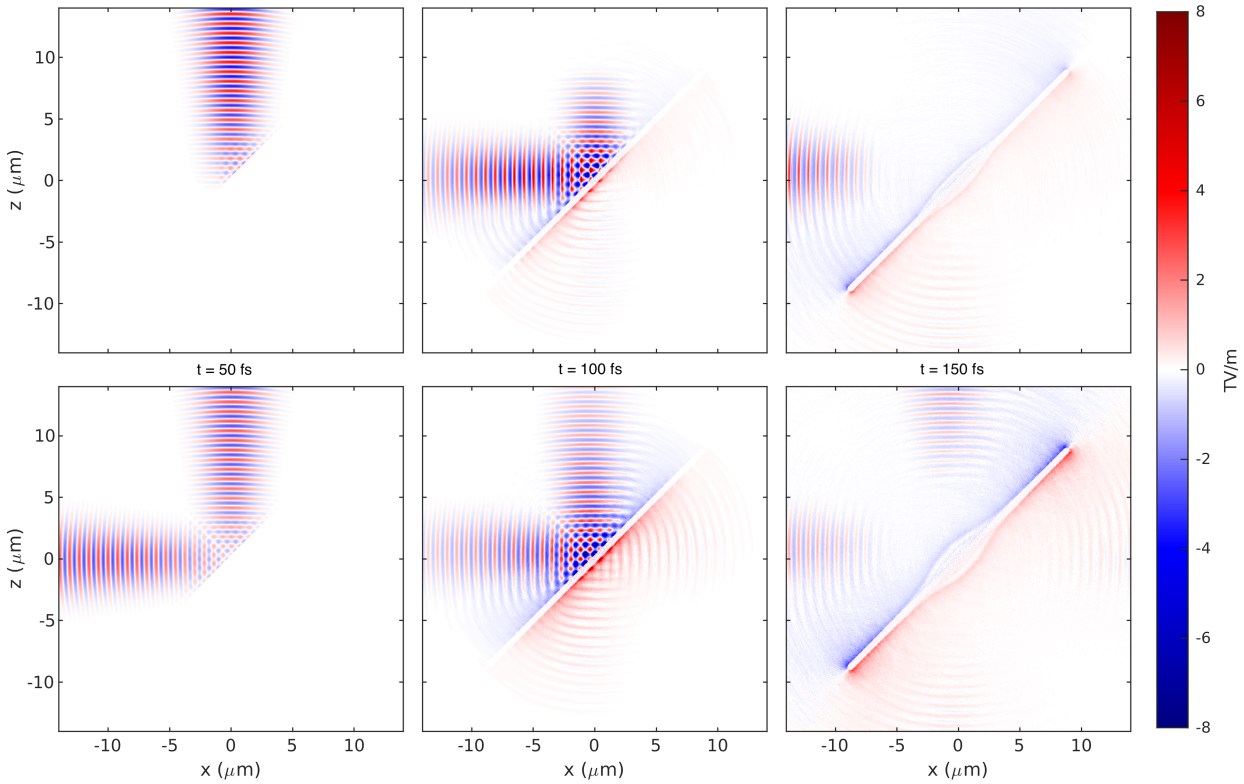

Figure 2.1: Electric field component normal to the target and in the plane of the simulation grid for the single pulse simulation (top panels) and double pulse simulation (bottom panels) at 50 fs (left panels), 100 fs (center panels), and 150 fs (right panels).

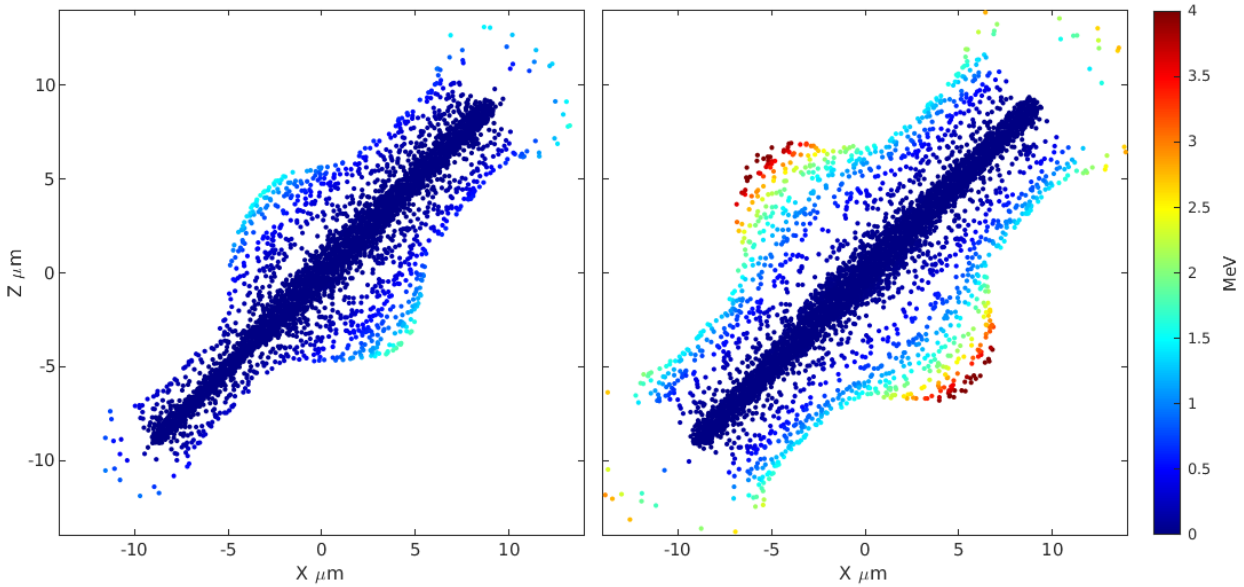

Figure 2.2: Proton energy 450 fs after pulse for single pulse (left panel) and double pulse (right panel).

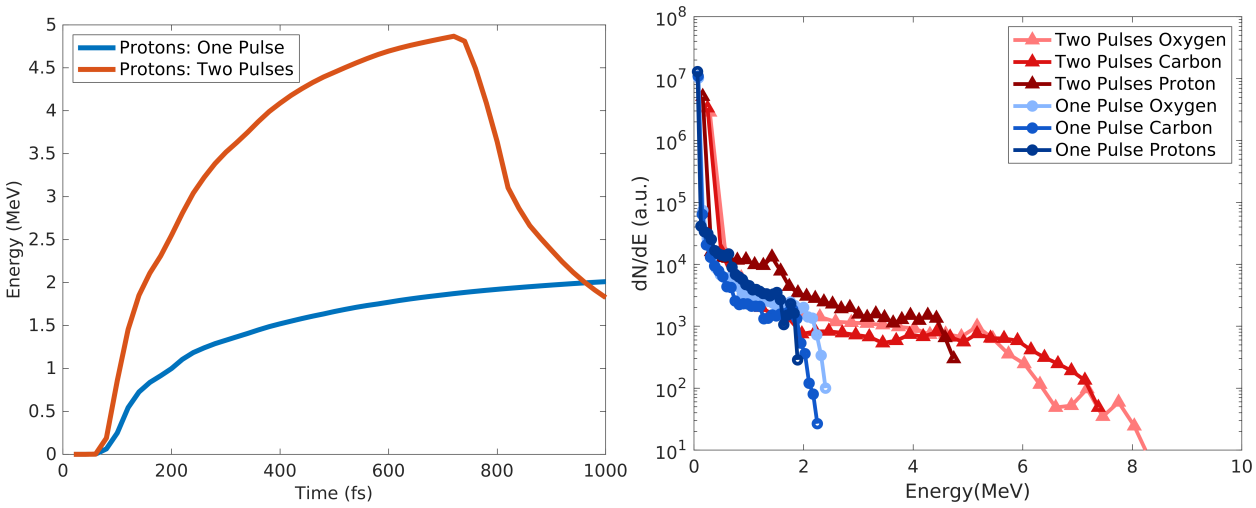

Figure 2.3: (left panel) Average energy over time of the 1000 most energetic proton macroparticles in the single pulse and double pulse simulations. (right panel) Comparing ion spectra at 700 fs after the start of the simulation.

The left panel of Fig. 2.3 illustrates how the maximum proton energy changes over time by displaying the average energy of the top 1,000 protons in the simulation. This figure shows that not only is there a a higher peak proton energy for the double pulse set up, but there is also a sharper increase in the maximum ion energy. The average of the top 1000 protons was shown here in order to achieve a smoother function over time as the highest energy protons are leaving the simulation. At 700 fs after the start of the simulation, the top 1,000 protons had an average energy of 1.85 MeV for the single pulse simulation and 4.84 MeV for the double pulse simulation. This remarkably shows an increase of 2.9 times greater proton energy for the double pulse simulation, despite both simulations having the same total pulse energy.

The right panel of Fig. 2.3 shows the ion spectra for both simulations at 700 fs into the simulation. These spectra show the maximum proton energy is increased from $\sim$2 MeV for the single pulse to $\sim$5.5 MeV for the double pulse simulation. This figure also shows that the number of energetic protons and ions is also increased through the entire spectra, and that this phenomena is not exclusive to only the highest energy ions.

2.4 Results from spatially or temporally offset pulses

Previous exploration of this effect have all involved pulses which are perfectly aligned both spatially and temporally. However, aligning two beams with such high precision can be challenging in experimental demonstration. Shot-to-shot variations can also lead to inconsistencies in the pulse alignment. Because of this, it is important to explore how closely the two beams must overlap both spatially and temporally. This section explores 2D3v simulations that have the same set up as the previous section, but with temporal, spatial, offsets.

The top left panel of Fig. 2.4 shows the effect of temporal offsets on the maximum ion energy at 750 fs after the start of the simulation. Here, temporal offset means that one of

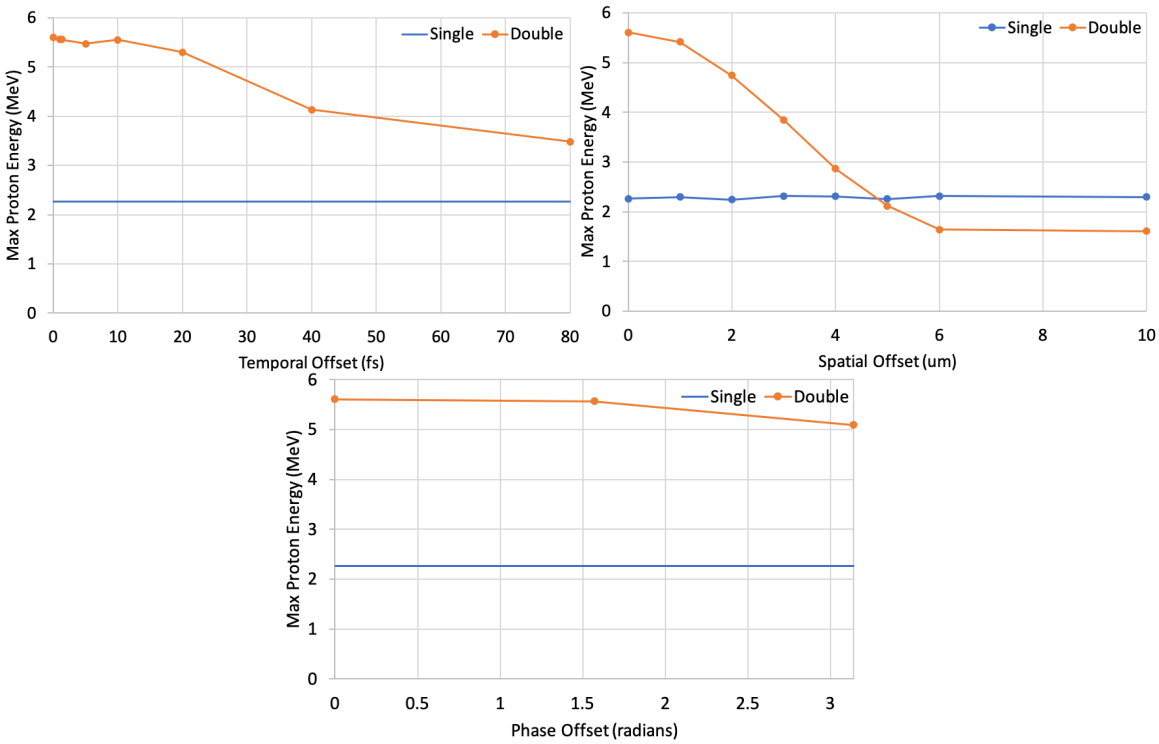

Figure 2.4: Maximum proton energy at 750 fs after the start of the simulation for various temporal offsets (top left), spatial offsets (top right), and phase offsets (bottom). The top left panel shows temporal offsets ranging from 1 fs to 80 fs. The double pulse simulations had one pulse delayed and the other pulse with no delay. The maximum proton energy for the single pulse simulation is shown with a horizontal line. The top right panel shows spatial offsets ranging from 1 µm to 10 µm. The bottom panel shows phase offsets ranging from 0 to π radians.

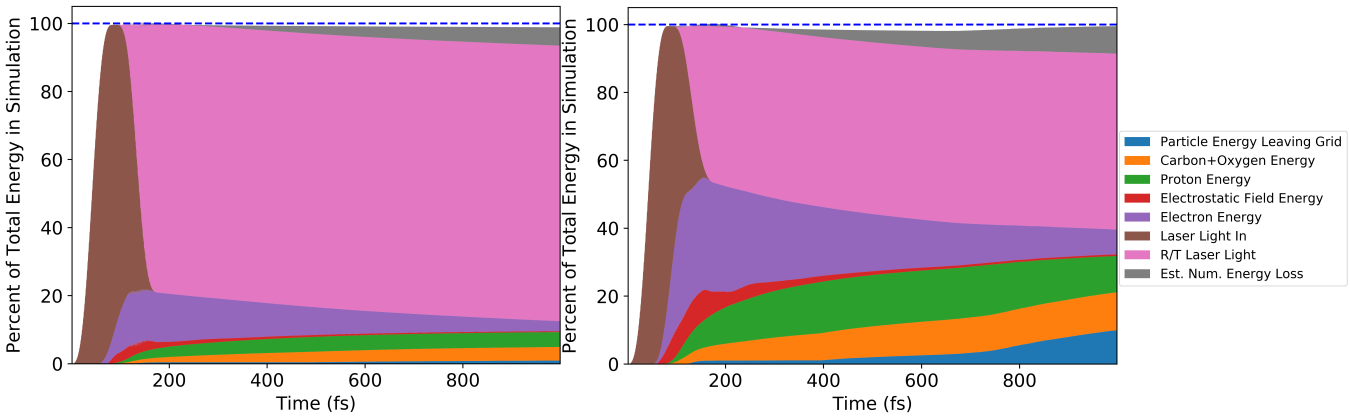

Figure 2.5: Evolution of various sources of energy in the Single Pulse (left panel) and Double Pulse (right panel) simulations. A horizontal dashed line shows the analytically derived total laser energy that enters the simulation. The LSP code includes a reliable estimate of energy loss due to numerical effects which is shown on the plot. Also included is an estimate of the laser energy that leaves the simulation through reflection or transmission. The lines do not all add up to 100% at late times only because electrons and protons ejected from the target eventually leave the simulation boundary.

the beams had a time delay. Interestingly, this figure shows that even when one pulse is delayed by 80 fs, there is still a noticeable increase in ion energy when using the double pulse configuration, despite the delay being nearly the full width full max laser pulse duration. This result may be similar to studies where two pulses arrived at the same angle, but with a time delay.

The top right panel of Fig. 2.4 shows the effect of spatial offsets on the maximum ion energy at 750 fs after the start of the simulation. Both beams were moved evenly away from the center of the target while keeping the focus on the target and without changing the angle of incidence. Both the single and double pulse beam positions were further adjusted to account for any fluctuations caused by the peak intensity being nearer to the edge of the target. The x-axis represents distance between the peak focus of the two beams in the case or the double pulse simulation, or twice the distance from the center of the target to the focus of the beam in the case of the single pulse simulations. Both upper panels show a decrease in peak ion energy as the two beams are further from perfect temporal and spatial alignment.

The bottom panel of Fig. 2.4 shows the effect of phase offsets on the maximum ion energy at 750 fs after the start of the simulation. No significant change is seen despite the phase offset.

2.5 Analysis and Discussion

Our simulations show significantly increased ion energy when using the double pulse configuration as described in Ferri, Siminos, and Fülöp [4] and Ferri et al. [5]. We saw

similar increases in the maximum ion energy and throughout the entire spectra of the ions. To explore further as to why this phenomena occurs, we investigate into the evolution of the various forms of energy in this simulation in Fig. 2.5.

Fig. 2.5 shows how energy is evolved through time for both the single pulse and the double pulse simulation. The energies are shown as a percentage of the total simulation energy, which is the same for both simulations. At earlier times in the simulation, the same laser energy enters the grid and the energies are similar for both simulations. As more laser energy is absorbed as electron energy for the double pulse simulation. 21% of the laser energy is converted into electron energy in the single pulse simulation, compared with 53% for the double pulse configuration. This is a striking difference of 2.25 times greater energy absorption. This increased electron energy then leads to a greater electrostatic field energy, which is then transferred into a greater ion energy for the double pulse configuration. Thus we conclude that an experimental demonstration with the double pulse configuration is expected to have a significant increase in absorption and a decrease in reflected and transmitted light.

In order to predict the behavior of this phenomena in an experimental demonstration, we observe how various spatial and temporal offsets affect the maximum ions in these simulations. The results in Sec. 2.4 show that a significant increase remains even when the pulses are offset spatially and temporally. These results show that even when the offset is approaching the full duration of the pulse (leading to very little constructive interference between the pulses) there is still a noticeable enhancement in ion energy. These results also show that an enhancement remains for pulses that are offset spatially by a distance larger that the beam spot size of the pulses. This leads us to conclude that experimental demonstration of this effect is feasible given the range of offsets which continue to provide substantial enhancement in ion energy.

2.6 Conclusion

From 2D3v PIC simulations we explore a configuration for double pulse enhanced TNSA, as described by Ferri, Siminos, and Fülöp [4]. We investigate if this configuration would be feasible for experimental demonstration on a milliJoule class laser system. We simulated a laser with lower intensity than that describe in Ferri, Siminos, and Fülöp [4] and with a thinner target of a different material. Despite the differences in simulation parameters, we still observed a significant increase in the maximum ion energy when comparing two pulses of half intensity ($2.5 * 10^18$ W cm^{-2}) to one pulse of at full energy ($5 * 10^18$ W cm^{-2}). We also examine the effect of spatial or temporal misalignment of the two laser pulses or phase differences on the maximum proton energy. Our simulations lead us to the conclusion that a laser system of this intensity should be able to demonstrate double pulse enhanced TNSA, which will be insightful for demonstration the effecr on much higher intensity laser systems.

Bibliography

[1] M. V. Ammosov, N. B. Delone, and V. P. Krainov. "Tunnel ionization of complex atoms and of atomic ions in an alternating electromagnetic field". In: *Sov. Phys. JETP* 64.December 1986 (1986), pp. 1191–1194. ISSN: 0044-4510. DOI: 10.1117/12.938695.

[2] S. V. Bulanov and V. S. Khoroshkov. "Feasibility of using laser ion accelerators in proton therapy". In: *Plasma Physics Reports* 28.5 (May 2002), pp. 453–456. ISSN: 1562-6938. DOI: 10.1134/1.1478534. URL: https://doi.org/10.1134/1.1478534.

[3] Antoaneta Ene, Ion V Popescu, and Claudia Stihi. "Applications of proton-induced X-ray emission technique in materials and environmental science". In: *Ovidius Univ Ann Chem* 20.1 (2009), pp. 35–39.

[4] J. Ferri, E. Siminos, and T. Fülöp. "Enhanced target normal sheath acceleration using colliding laser pulses". In: *Communications Physics* 2.1 (Apr. 2019), p. 40. ISSN: 2399-3650. DOI: 10.1038/s42005-019-0140-x. URL: https://doi.org/10.1038/s42005-019-0140-x.

[5] J. Ferri et al. "Effects of oblique incidence and colliding pulses on laser-driven proton acceleration from relativistically transparent ultrathin targets". In: *Journal of Plasma Physics* 86.5 (2020), p. 905860505. DOI: 10.1017/S0022377820000847.

[6] IP Jain and Garima Agarwal. "Ion beam induced surface and interface engineering". In: *Surface Science Reports* 66.3-4 (2011), pp. 77–172.

[7] Alex Russell and Douglass Schumacher. "Extending the binary collision algorithm to non-Spitzer systems and application to laser heating and damage". In: *Physics of Plasmas* 24.8 (2017), p. 080702.

[8] Yousef I. Salamin, Zoltán Harman, and Christoph H. Keitel. "Direct High-Power Laser Acceleration of Ions for Medical Applications". In: *Phys. Rev. Lett.* 100 (15 Apr. 2008), p. 155004. DOI: 10.1103/PhysRevLett.100.155004. URL: https://link.aps.org/doi/10.1103/PhysRevLett.100.155004.

[9] R. A. Snavely et al. "Intense High-Energy Proton Beams from Petawatt-Laser Irradiation of Solids". In: *Phys. Rev. Lett.* 85 (14 Oct. 2000), pp. 2945–2948. DOI: 10.1103/PhysRevLett.85.2945. URL: https://link.aps.org/doi/10.1103/PhysRevLett.85.2945.

[10] Xiufang Tian et al. "The evolution of proton beam therapy: Current and future status". In: *Molecular and clinical oncology* 8.1 (2018), pp. 15–21.

[11] D. R. Welch et al. “Integrated simulation of the generation and transport of proton beams from laser-target interaction”. In: *Physics of Plasmas* 13.6 (June 2006), p. 063105. DOI: 10.1063/1.2207587.

[12] SC Wilks et al. “Energetic proton generation in ultra-intense laser–solid interactions”. In: *Physics of plasmas* 8.2 (2001), pp. 542–549.